Polymeric Nonelectrolytes to Probe Pore Geometry: Application to the α-Toxin Transmembrane Channel

Petr G. Merzlyak,*# Liliya N. Yuldasheva,* Cláudio G. Rodrigues,* Carlos M. M. Carneiro,* Oleg V. Krasilnikov,*# and Sergey M. Bezrukov§¶

*Laboratory of Membrane Biophysics, Department of Biophysics and Radiobiology, Federal University of Pernambuco, 50670-901, Recife, PE, Brazil; #Laboratory of Molecular Physiology, Institute of Physiology and Biophysics, 700095 Tashkent, Uzbekistan; §Laboratory of Physical and Structural Biology, National Institute of Child Health and Human Development, National Institutes of Health, Bethesda, Maryland 20892 USA; and ¶St. Petersburg Nuclear Physics Institute, Gatchina 188350, Russia

ABSTRACT Asymmetrical (one-sided) application of penetrating water-soluble polymers, polyethylene glycols (PEGs), to a well-defined channel formed by *Staphylococcus aureus* α-toxin is shown to probe channel pore geometry in more detail than their symmetrical (two-sided) application. Polymers added to the *cis* side of the planar lipid membrane (the side of protein addition) affect channel conductance differently than polymers added to the *trans* side. Because a satisfactory theory quantitatively describing PEG partitioning into a channel pore does not exist, we apply the simple empirical rules proposed previously (Krasilnikov et al., 1998, *J. Membr. Biol.* 161:83–92) to gauge the size of pore openings as well as the size and position of constrictions along the pore axis. We estimate the radii of the two openings of the channel to be practically identical and equal to 1.2–1.3 nm. Two apparent constrictions with radii of $\sim$0.9 nm and $\sim$0.6–0.7 nm are inferred to be present in the channel lumen, the larger one being closer to the *cis* side. These structural findings agree well with crystallographic data on the channel structure (Song et al., 1996, *Science.* 274:1859–1866) and verify the practicality of polymer probing. The general features of PEG partitioning are examined using available theoretical considerations, assuming there is no attraction between PEG and the channel lumen. It is shown that the sharp dependence of the partition coefficient on polymer molecular weight found under both symmetrical and asymmetrical polymer application can be rationalized within a "hard sphere nonideal solution model." This finding is rather surprising because PEG forms highly flexible coils in water with a Kuhn length of only several Angstroms.

INTRODUCTION

Ion channels are usually composed of one or a few integral membrane proteins surrounding a central water-filled pore. Pore geometry is crucial. Together with the fixed charge distribution, it mainly defines conductance, selectivity, and other transport properties of the channel. While electron microscopy and x-ray diffraction are the primary methods used for determination of channel structure, multiple difficulties inherent in these methods restrict their accuracy. Most importantly, in both methods channels can be significantly distorted either by fixing proteins to a surface or by assembling them into a crystal. In contrast, electrophysiological methods reveal conductance and selectivity of channels under conditions that are very close to those in vivo and thus give additional important information about the properties of a channel lumen in its native states (Hille, 1992). This information can be further enhanced by combining electrophysiological measurements with new physical methods developed to probe channel structure. Among the newer approaches is the use of water-soluble neutral polymers (Zimmerberg and Parsegian, 1986; Sabirov et al., 1991, 1993; Krasilnikov et al., 1992; Vodyanoy and Bezrukov, 1992; Bezrukov and Vodyanoy, 1993; Parsegian et al., 1995; Villarroel et al., 1995; Bullock and Kolen, 1995; Korchev et al., 1995; Bezrukov et al., 1996; Bezrukov and Kasianowicz, 1997; Desai and Rosenberg, 1997; Kaulin et al., 1998; Ternovsky and Berestovsky, 1998).

A novel refinement of the polymer exclusion method (Sabirov et al., 1991, 1993; Krasilnikov et al., 1992) suggests that not only can the size of each channel opening be estimated, but that the presence, size, and apparent localization of structural constrictions inside an ion channel water pore can also be inferred (Krasilnikov et al., 1998). The method relies on the effect of asymmetrically applied polymeric nonelectrolytes on channel conductance to estimate parameters of channel pore geometry. Here we test the validity of such an interpretation with a heptameric transmembrane channel formed by *Staphylococcus aureus* α-toxin (α-hemolysin) in a planar lipid bilayer. This channel is chosen because its structure has been determined to 0.19-nm resolution (Song et al., 1996), and it is well studied electrophysiologically, including a number of estimations of its pore size in biological and model membranes.

Staphylococcus aureus α-toxin is a 293-residue single-chain protein with a molecular mass of 33.2 kDa (Grey and Kehoe, 1984). In a native form it is a water-soluble monomer that undergoes conformational transformation during membrane binding and subsequent insertion, assembly, and pre-pore and pore formation (Valeva et al., 1996; Vecsey-Semjen et al., 1997; Tomita et al., 1992). The ability of this toxin to form ion channels in lipid bilayers was discovered some 20 years ago (Krasilnikov et al., 1980, 1981). It is

Received for publication 11 May 1999 and in final form 30 August 1999.

Address reprint requests to Dr. Sergey M. Bezrukov, National Institutes of Health, Bldg. 9, Room 1E-122, Bethesda, MD 20892-0924. Tel.: 301-402-4701; Fax: 301-402-9462; E-mail: bezrukov@helix.nih.gov.

0006-3495/99/12/3023/11 $2.00

generally accepted now that transmembrane pore formation is a main mechanism by which α-toxin damages target cells. Seven molecules of α-toxin form the transmembrane channel (Gouaux et al., 1994).

The apparent radius of the channel pore was originally inferred (Bhakdi et al., 1984; Walev et al., 1993; Jonas et al., 1994; Menestrina, 1986; Krasilnikov et al., 1988; 1992; Korchev et al., 1995; Bezrukov et al., 1996; Bezrukov and Kasianowicz, 1997) to be in the 0.5–1.4-nm range in biological membranes and in the 0.5–1.3-nm range in lipid bilayers. More recently, an x-ray diffraction study of a crystal form of α-toxin heptamers (Song et al., 1996) showed that the pore is a solvent-filled channel, 10 nm in length, with a radius changing from 0.7 nm to 2.3 nm.

Here we present evidence that further demonstrates the capabilities of the polymer-probing approach. We compare the channel geometry deduced from the polymer-induced changes in α-toxin channel conductance for asymmetrical polymer application with the geometry obtained from the crystallographic data. As we discuss in the concluding section, the physics of polymer partitioning in the channel pore is not well understood, even in the case of symmetrical (equilibrium) polymer application. Nevertheless, remarkably, by applying simple empirical rules to single-channel conductance data, we deduce several features of pore geometry that are in good agreement with the crystallographic data of Song et al. (1996). We find that while radii of the channel openings at both ends are nearly equal (1.2–1.3 nm), the pore size changes asymmetrically along the pore axis, with two apparent constrictions of $\sim$0.9 nm and $\sim$0.6–0.7 nm radii.

Recently, an atomic force microscopy study by Czajkowsky et al. (1998) gave evidence for a hexameric stoichiometry of α-toxin channels in phospholipid bilayers. These authors conclude that α-toxin can form two different energetically stable oligomers. It would be tempting to apply our technique to discriminate between the two. Unfortunately, the direct comparison of the structural features of the pore deduced from polymer probing described here with the hexamer pore is problematic because oligomers of different size may differ by the subunit structure as well (Czajkowsky et al., 1998).

MATERIALS AND METHODS

Staphylococcus aureus α-toxin was a generous gift of Dr. K. D. Hungerer (Behringwerke Laboratories, Marburg, Germany) and Dr. H. Bayley (Texas A&M University). Pure phosphatidylcholine (Type V-E) and cholesterol were purchased from Sigma. The polymeric nonelectrolytes were polyethylene glycols (PEGs) of different molecular weights: PEG200, PEG300, and PEG400 (Sigma); PEG600 (Riedel de Haen); PEG1000 and PEG1450 (Sigma); PEG2000 and PEG3000 (Loba Chema); and PEG3400 and PEG4600 (Sigma). Polymers were additionally purified by anion-exchange chromatography, using strong alkaline anion exchangers (III or IV; Merck) to remove contaminants that decrease the stability (lifetime) of black lipid membranes and increase the probability of ion channel transitions from open to closed states. Other chemicals were analytical grade and were used without additional purification.

Hydrodynamic radii of nonelectrolytes established in previous studies (Sabirov et al., 1991, 1993; Krasilnikov et al., 1992) are as follows: 0.43 $\pm$ 0.03 nm for PEG200; 0.6 $\pm$ 0.03 nm for PEG300; 0.7 $\pm$ 0.03 nm for PEG400; 0.8 $\pm$ 0.04 nm for PEG600; 0.94 $\pm$ 0.03 nm for PEG1000; 1.05 $\pm$ 0.03 nm for PEG1450; 1.22 $\pm$ 0.03 nm for PEG2000; 1.44 $\pm$ 0.03 nm for PEG3000; 1.63 $\pm$ 0.03 nm for PEG3400; and 2.1 $\pm$ 0.03 nm for PEG4600. These values are in good agreement with the "equivalent sphere radii" obtained by a quite different method, size exclusion chromatography (Kuga, 1981), e.g., 1.27 nm for PEG 2000. They are also in accord with the results on PEG hydrodynamic radii deduced from diffusion coefficients by Couper and Stepto (1969). Using their result for PEG1540 and correcting it by a factor of $(2000/1540)^{3/5}$, we obtain 1.31 nm for PEG2000.

Bilayer lipid membranes (BLMs) were formed at room temperature (25 $\pm$ 2°C) by the method of Mueller (Mueller et al., 1963) from a phosphatidylcholine-cholesterol mixture (3:1, by mass). A 2% lipid solution in *n*-decane was used to form bilayers. Double-distilled water was used to prepare all buffer solutions. Unless stated otherwise, the standard solution used in the bilayer experiments contained 0.1 M KCl and 5 mM Tris at pH 7.5 adjusted with 1.0 M citric acid. To keep the ion/water molar ratio constant, polymers were added to the standard KCl solution to 20% (w/v) concentration. The conductivity of each solution was measured with a HI 9033 (HANNA Instruments) multirange conductivity meter at 25°C. Experiments were carried out under voltage-clamp conditions. The *trans* compartment was connected to virtual ground through an operational amplifier in current-to-voltage configuration. Negative ($-$40 mV) voltages were applied to the *cis* compartment of the chamber on the side of the α-toxin addition.

A final concentration of α-toxin was $\sim$4 ng/ml. Current signals were monitored with a storage oscilloscope (model 201; Nicolet Instrument Corporation) and recorded with a strip chart recorder (Hewlett Packard 70158 X-Y Recorder). Current traces were read by hand, and single-channel conductances were estimated by dividing the single-channel current by the applied transmembrane voltage. Histograms of the events under all experimental conditions demonstrated a large main pool and two relatively small pools of conductance steps. The least-squares method with a minimum random search algorithm (Eler, 1972) was used to characterize the histograms by a sum of three normal distributions. The mean value of the main pool of the channel conductance obtained as the best approximation was used for the subsequent analysis.

To estimate the size of two openings of an ion channel as well as the presence and the apparent localization of constrictions inside an ion channel water lumen, a recently developed empirical approach (Krasilnikov et al., 1998) was used. The filling of a single channel by differently sized polymeric nonelectrolytes from the *cis* (that is, the side of toxin addition) and from the *trans* opening was examined in separate experiments. Differently sized polymers were applied from one side of the membrane, while the impermeant large polymer (PEG4600) was added to the other.

To deduce pore structural features we introduce the polymer filling factor, $F(w)$, which describes the ratio of the pore length that is accessible to a polymer of a given molecular weight, w, to the total pore length L. Under equilibrium conditions (symmetrical application of polymers) a filling factor of 1.0 would correspond to equipartitioning, that is, to a large pore in the presence of small polymers that occupy all of the volume of the pore with a concentration equal to that in the bulk. It should be stated here that even under equilibrium conditions there is no reliable theory that describes partitioning quantitatively when the sizes of the pore and the polymer are comparable. In the particular case of PEG/α-toxin channel, partitioning can be complicated by direct polymer/pore interactions (Bezrukov et al., 1996; Bezrukov and Kasianowicz, 1997), as has been seen in recent measurements of attractive forces between proteins and end-grafted PEG chains (Sheth and Leckband, 1997). A further complication is that with the asymmetrical PEG application used in the present study, polymer partitioning is nonequilibrium in nature, e.g., there is a net flux of polymers through the pore. For these reasons, to estimate the filling

factor $F(w)$, we will use several strong simplifying assumptions. We will assume that

1. The effect of polymers on bulk electrolyte conductivity and pore conductance is the same and can be related to the average polymeric concentration in the bulk and in the pore.

2. Polymers that are smaller than the pore opening fill the pore to the same concentration as in the bulk all the way to a constriction and do not fill any of the pore behind the constriction if the constriction radius is smaller than the polymer hydrodynamical radius.

3. The deviation of the pore shape from a simple regular cylinder is much more significant for polymer partitioning than for the pore geometrical conductance factor per se. That is, rather than solving the following inverse problem of finding the pore radius $r(x)$ as a function of coordinate x along the pore axis from pore conductance, $g(w)$, in the presence of polymers of different molecular weight, w,

$$g(w) = \pi\left(\int_0^L \frac{dx}{r^2(x)\chi(w, x)}\right)^{-1}, \qquad (1M)$$

where L is the pore length and $\chi(w, x)$ is the local electrolyte conductivity, which depends on both polymer weight and coordinate, we simplify the problem as follows. Using assumption 2 and considering the changes in $\chi(w, x)$ to be much larger than changes in $r^2(w)$, we write

$$g(w) = \frac{\pi r^2}{L}\left(\frac{F(w)}{\chi(w)} + \frac{1 - F(w)}{\chi_0}\right)^{-1}, \qquad (2M)$$

where $\chi(w)$ is the solution conductivity of the polymer-accessible part of the pore, χ_0 is the solution conductivity in the absence of polymers (for the solution that fills the part of the channel that is polymer-inaccessible), and r is the effective pore radius. If g_0 is the channel conductance in the presence of impermeant polymers, $g_0 = \pi r^2\chi_0/L$, then from Eq. 2M we obtain (Krasilnikov et al., 1998)

$$F(w) = \frac{(g_0 - g(w))\chi(w)}{(\chi_0 - \chi(w))g(w)}. \qquad (3M)$$

All three simplifications that we adopt here are severe. However, as will be shown below, they allow us to deduce several conclusions about the α-toxin channel pore geometry that are in surprisingly good agreement with the x-ray structural data.

The first assumption seems to be the least restrictive one. At the same time it is worth mentioning that the detailed quantitative mechanism by which water-soluble polymers decrease electrolyte solution conductivity is not understood (Berezhkovskii et al., 1999). Several complications (e.g., due to the pore-induced change in polymer configuration/orientation in comparison to the bulk) are easily envisioned. The second assumption is severe, indeed. It is quite clear that it generally does not hold, even for hard spheres (hard sphere partitioning is very sensitive to the size of the cavity and is greatly reduced if the sphere radius is close to the cavity size). We will return to this in the concluding section of the Discussion. The third assumption is very strong too, but, in our opinion, in the absence of any theoretical work in this direction, it is justified as a starting point.

Additional complications include corrections for the PEG-induced changes in ion activity (e.g., the single-channel conductance, g_o, should be measured in the polymer-free solution with the electrolyte concentration increased to account for PEG-bound water) and for the access resistance, as was done for the equilibrium partition coefficient with symmetrical polymer application (Bezrukov and Vodyanoy, 1993; Bezrukov et al., 1996; Krasilnikov et al., 1998). These two effects are ignored here because they are small and partially compensate for each other and, therefore, do not influence the deduced filling factor substantially.

RESULTS

Channel conductance in the presence of PEG at one of its openings

When α-toxin was added to the aqueous phase bathing a bilayer lipid membrane, stepwise increases in current were observed (Fig. 1, *inset*). These steps reflect the formation of individual channels. At pH 7.5 most of these conductance steps were directed upward; the downward steps corresponding to channel closing events were detected only rarely at a transmembrane voltage of −40 mV. The histogram shown in Fig. 1 represents the conductance step values for these unitary events. It is seen that channel conductance is nonuniform. The most frequent value was observed in the range of 80–120 pS. The small lower pools could be a reflection of noncomplete opening of the channel or/and slight (invisible in Coomassie-stained 10% polyacrylamide gels run in the presence of sodium dodecyl sulfate; data not shown) contamination of nicked toxin, which usually forms a low-conductance channel (Krasilnikov et al., 1997). These low-conductance pools were ignored and were not analyzed further. The mean value of the single-channel conductance in the main pool was determined to be 107.5 ± 3.2 pS (0.1 M KCl) and was used in the subsequent analysis.

To gauge the size of each entrance of the α-toxin channel and to probe the geometry of the channel lumen, we measured the channel conductance with polymeric nonelectrolytes added to the *cis* or *trans* side of the membrane. These two additional groups of histograms were analyzed analogously to the control in Fig. 1. Mean conductances of the main pools in the presence of a test polymer on the *cis* (g^{cis}) or *trans* (g^{trans}) side of the channel are presented in Table 1. To complete the data set, we also include the values of the channel conductance in the presence of polymers on both sides of the membrane (g^{both}).

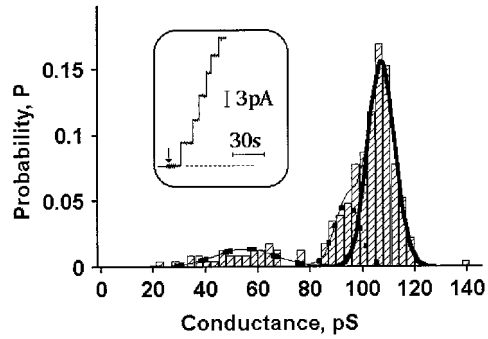

FIGURE 1 The amplitude histogram of conductance steps induced by α-toxin in voltage-clamped (−40 mV) phosphatidylcholine-cholesterol (1:1, by mass) membranes formed by the method of Mueller et al. (1963) in 0.1 M KCl, 0.005 M Tris-citrate (pH 7.5). The bin width is 6 pS. More than 200 events were observed (five to seven channels per membrane). Protein was added to the *cis*-compartment. The single-channel conductance distribution was fitted with a sum of three normal distributions (*fine line*). The mean value of the main pool (*heavy line*) was used in our analysis. A typical single-channel recording is shown in the inset. The dashed line indicates the zero current level, and the arrow shows the addition of the toxin to a final concentration of 1–2 nM.

TABLE 1 Channel conductance and solution conductivity (0.1 M KCl) as changed by PEG addition

		χ (mS/cm)	r (nm)	g^{both}, N_i (N)	V_{rev} (mV)	g^{cis}, N_i (N)	g^{trans}, N_i (N)
1	Control	12.95		107.5 ± 3.1; 157 (230)			
2	Glycerol	7.10	0.308	55.1 ± 6.5; 106 (228)	3.5 ± 0.7	71.6 ± 3.7; 120 (213)	72.7 ± 5.6; 129 (234)
3	PEG200	6.15	0.430	49.4 ± 3.6; 328 (405)	2.6 ± 0.6	69.1 ± 5.3; 175 (311)	65.0 ± 5.2; 310 (473)
4	PEG300	6.00	0.600	50.0 ± 7.4; 191 (265)	1.9 ± 0.4	75.8 ± 5.5; 225 (469)	52.5 ± 5.0; 207 (278)
5	PEG400	5.92	0.700	53.1 ± 5.7; 214 (431)	1.6 ± 0.3	75.1 ± 3.7; 40 (5)	68.9 ± 3.9; 63 (156)
6	PEG600	5.95	0.780	57.9 ± 3.5; 74 (157)	1.5 ± 0.3	75.1 ± 5.1; 185 (464)	69.0 ± 3.2; 95 (340)
7	PEG1000	5.72	0.940	59.0 ± 5.1; 141 (184)	1.0 ± 0.2	75.9 ± 5.8; 115 (475)	73.7 ± 7.4; 263 (465)
8	PEG1450	5.70	1.050	68.7 ± 5.2; 190 (218)	0.5 ± 0.2	81.5 ± 5.1; 112 (212)	83.1 ± 4.4; 136 (443)
9	PEG2000	5.71	1.220	91.9 ± 6.0; 300 (371)	0.3 ± 0.2	100.0 ± 4.8; 141 (163)	104.2 ± 6.5; 108 (142)
10	PEG3000	5.73	1.440	105.6 ± 3.2; 121 (361)	0.3 ± 0.1		
11	PEG3400	5.66	1.630	105.3 ± 4.4; 155 (204)	0.0	105.5 ± 4.2; 136 (179)	104.6 ± 7.6; 97 (154)
12	PEG4600	5.65	2.100	106.4 ± 7.3; 141 (220)	0.0	106.4 ± 7.3; 141 (220)	106.4 ± 7.3; 141 (220)

χ (mS/cm), solution conductivities measured with accuracy of ±0.5%; r (nm), hydrodynamic radii of nonelectrolytes obtained by viscometry (Sabirov et al., 1991; 1993; Krasilnikov et al., 1992). V_{rev} (mV), transmembrane potentials appearing at a zero current through the system when a given PEG (or glycerol) was in contact with one of the channel openings while the other opening was in contact with PEG4600. The sign was positive in the PEG4600-containing compartment. Single-channel conductances (pS) are expressed as mean ± SD. N_i is the number of the single channel events counted in the main pool that was obtained from the computer analysis of the histogram as described in Materials and Methods. N is the number of the single channel events counted in the whole histogram. g^{both} was obtained in the presence of the same nonelectrolyte at both sides of the bilayer; g^{cis} was measured in the presence of a given nonelectrolyte at the *cis*-side of the bilayer while PEG4600 was present at the *trans*-side, and g^{trans} refers to the conductance measured in the presence of a given nonelectrolyte at the *trans*-side of the bilayer while PEG4600 was present at the *cis*-side. Because of the presence of V_{rev} in those asymmetric system, g^{cis} and g^{trans} were calculated as follows: $g^{cis} = I_{ch}/(V_m + V_{rev})$; $g^{trans} = I_{ch}/(V_m - V_{rev})$, where I_{ch} is the value of the current passing through the channel; V_m is the voltage difference applied to lipid bilayers.

One can see that for PEGs with molecular weights smaller than 1000, g^{cis} is always larger than g^{trans}. Two conclusions can be drawn from this observation. First, α-toxin channels insert not in a random but in an oriented manner. A similar conclusion was reached much earlier from analysis of single-channel current-voltage curves exhibiting a significant asymmetry in a certain pH range (Krasilnikov and Sabirov, 1989). Second, this indicates an asymmetry in the structure of the channel water pore. Starting from the smallest PEGs (PEG200 and PEG300), an increase in PEG hydrodynamic radius leads to a regular increase in g^{cis} as well as g^{trans}. The PEG size at which the polymer-induced effect saturates is close to PEG2000 in both cases. Thus the "cutoff" size for polymer penetration into the channel pore is about the same for the two openings, indicating that the radii of the two α-toxin channel openings are very similar.

While the data presented in Table 1 can be used directly to estimate the apparent sizes of the channel entrances, we will rather analyze the dependence of pore filling on polymer hydrodynamic radius. The filling of the channel pore with polymers presented in Fig. 2 was calculated from the channel conductance as described in Materials and Methods. As expected, the filling, F, is dependent on the hydrodynamic radius of polymer molecules. In both cases maximum values of F, observed in the presence of the smallest nonelectrolyte, are close to 0.6. In this case there is no constriction inside the channel lumen that is narrow enough to stop the flux of glycerol molecules through the pore. It is natural to expect that the average concentration of glycerol in the pore would be half of that in the bulk, so that the formal application of Eq. 3M would give 0.5, which is close to the experimentally obtained value. When polymers with larger hydrodynamic radii were used, we observed significantly different values for F^{cis} and F^{trans}, indicating asymmetry in the α-toxin channel geometry. In both cases the dependence of filling on the hydrodynamic radius of PEG shows a biphasic behavior, which, in the case of a cylindrical geometry, suggests the presence of a constriction(s) in the channel lumen.

Geometrical features of the channel pore from *cis*- and *trans*-filling experiments

Because several theoretical issues concerning polymer partitioning into a channel pore are still unresolved, even in the

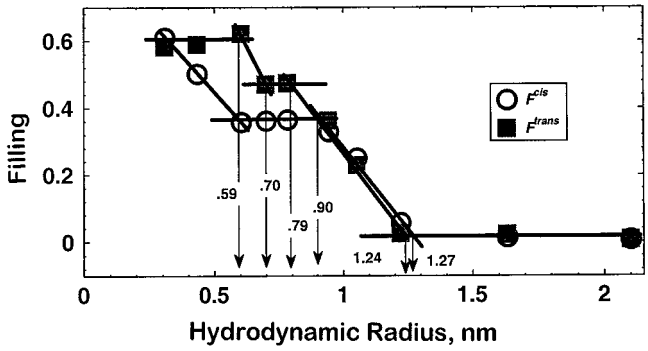

FIGURE 2 Dependence of F^{cis} (○) and F^{trans} (■) for asymmetrical addition of polymers to the *cis* and *trans* sides of the cell on polymer hydrodynamic radii. The values of F^{cis} and F^{trans} for each polymer were calculated as described in Materials and Methods. The error bars are equal to or smaller than the symbols used. Arrows indicate the radii values at critical points. Division of F^{cis} and F^{trans} dependences into plateau and slope segments was made by eye; these segments then were fitted by zero-order and first-order regressions, correspondingly.

case of symmetrical equilibrium conditions (see Materials and Methods and the last section of Discussion), in the following two sections we will follow a purely empirical approach (Krasilnikov et al., 1998).

In the *cis*-filling experiments the lowest level of filling ($F^{cis} \approx 0$) is observed for the largest PEG used. Molecules with radii larger than 1.22 nm do not enter the channel from the *cis* entrance at all. It can be seen (Fig. 2) that a decrease in polymer size leads to a progressive, but biphasic, increase in filling. This behavior suggests that the size of the channel pore does not change smoothly from *cis* to *trans* opening. Three straight lines can fit this part of the dependence (from *right to left*). The first line fits a pronounced slope observed for molecules, the radii of which varied from 0.9 nm to 1.22 nm. The second line fits a relatively long plateau of the dependence with $F^{cis} = 0.36$. The third line fits the slope of the dependence that is measured for molecules with sizes between those of glycerol and PEG300 ($r = 0.31–0.6$ nm) when filling increases from 0.36 to its maximum value of 0.6. For these small sizes there is a pronounced unidirectional flow of polymer molecules through the channel, partitioning is highly nonequilibrium, and, as a consequence, Eq. 2M is not applicable.

Based on our assumptions (see Materials and Methods), we argue that the interception between the first line that fits the slope of the falling part of F^{cis} dependence and its lowest invariant part ($F^{cis} \approx 0$) gives the radius (1.26 nm) of the channel *cis* opening. The interception between the first and second lines (0.9 nm) gives the radius of the first constriction as seen from the *cis* side opening. Polymers of this and smaller sizes fill the part of the pore between this and the second (with a smaller aperture) constriction, with partitioning independent of their size. Their size gets smaller than the aperture of the second constriction at the intersection of the second and third lines at 0.6 nm.

Thus we first deduce the decrease in the channel radius from ~1.25 nm to ~0.9 nm; then after this point, the radius stops decreasing until the main constriction ($r \approx 0.6$ nm) is reached. The presence of a relatively long intermediate invariant part of the dependence with $F^{cis} = 0.36$ means that molecules of PEG with hydrodynamic radii varying from 0.9 nm to 0.6 nm are equally effective in filling the channel pore. Their penetration along the pore axis is restrained by the major constriction. The relative position of this constriction, as seen from the *cis* side opening, can be approximately estimated by the ratio of filling value for this plateau and its maximum value (Krasilnikov et al., 1998) as $0.36/0.6 = 0.6$.

In the *trans*-filling experiments polymer partitioning also shows biphasic behavior (Fig. 2), although it is much less expressed. As in the case of *cis*-filling experiments (see above), molecules with radii larger than 1.22 nm do not enter the channel from the *trans* opening at all ($F^{trans} \approx 0$). Complete polymer exclusion from the pore is observed for almost the same PEGs as for the *cis*-filling. This demonstrates that the size of the *trans* opening is close to the size of the *cis* opening. Again, a decrease in polymer size leads to a progressive increase in filling. The decreasing part of the dependence can be divided into four regions approximated by four straight lines. The first (from *right to left*) line fits an extended slope observed for molecules, the radii of which varied from 0.8 nm to 1.22 nm. The interception between this line and the lowest invariant part of the dependence indicates the radius (1.24 nm) of the *trans* opening of the channel.

In the range of sizes between glycerol and PEG300 ($r = 0.31–0.6$ nm), for the reasons that we do not know, F^{trans} and F^{cis} differ qualitatively. While *cis*-filling still grows as probing molecule size decreases, *trans*-filling saturates to its maximum value at the size of PEG300. The biphasic features of the *trans*-filling are poorly expressed. Among the tentative conclusions would be the existence of the main constriction of 0.7 nm radius. Its position along the pore axis would be predicted as close to the *cis* opening of the pore because of the high filling value (>0.4) at this radius. However, if not for just one point (PEG600), the curve would be described by a simple, smooth transition between complete exclusion and maximum filling. Therefore, the reasoning applied above to the *cis*-filling data seems to be too risky in this case.

Summary of α-toxin channel probing with neutral polymers

Our simplified analysis of the single-channel conductance in the presence of polymeric nonelectrolytes allows us to conclude that radii of the two openings of the channel are practically equal and close to 1.2–1.3 nm. We also infer that the channel has a main constriction with a radius of ~0.6–0.7 nm. From the *cis*-filling experiments we predict the presence of the second constriction (with $r \approx 0.9$ nm), which is situated between the *cis* opening and the main constriction.

DISCUSSION

Probing with polymers versus crystallographic data

Let us compare our findings with crystallographic data on the channel structure (Song et al., 1996). The authors divide the channel structure into three domains, two of which, Cap and Stem, form the channel openings defined, respectively, as cis and trans in our study. The channel pore length is 10 nm and the radius of the *cis* opening is ~1.4 nm. At ~3.5 nm from the *cis* opening the channel pore reaches its maximum radius of 2.3 nm. The narrowest part of the pore, with a radius of ~0.7 nm, was established to be near the channel center. It was also found that in the stem region, the pore radius varies from 0.7 to 1.2 nm, depending on the volume of the side chains that protrude into the 1.3-nm-radius cylinder. Just from this description of the channel one can see a significant likeness with the geometrical features established in our study.

To make a detailed comparison, it is necessary to reconstruct the complete profile of the pore radius along the

channel axis. Data by Song et al. (1996) were used for the radius estimates in the following way. The sizes of the *cis* opening, widest and narrowest parts of the channel, were taken directly from Song et al. (1996). The radius of the stem region was calculated at 0.55-nm intervals along the channel axis, starting from the first side chains that protrude into the interior of the β-barrel stem. The 0.55-nm interval is equal to the distance between such neighboring side chains of the β-strands, which are tilted with respect to the barrel axis at $\sim$38°. For each point the radius was taken to be equal to the difference between the maximum value of the stem radius (measured from α-carbons of β-strands to the pore center) and the mean size of two side chains at this position. The size of the other part of the channel lumen was taken from analysis of the sagittal section of the channel presented by Song and co-authors in their figure 4. The final results of such analysis of the crystallographic structure of the α-toxin channel together with the geometrical features of the channel lumen obtained from our experiments are presented in Fig. 3. Constriction positions for the geometry deduced from polymer probing are taken to coincide with those obtained from the crystallographic data.

It could be seen that almost all of the structural features deduced from the polymer probing are in good accord with the crystallographic data. We have obtained a value for the radius of the *cis* opening equal to $\sim$1.3 nm, and it is 1.4 nm according to the crystallographic study. We have inferred that the minimum radius of the channel is 0.6–0.7 nm; this value is close to that obtained from the crystal structure. Both approaches show the presence of the intermediate constriction between the *cis* opening and the main constriction, with a radius $\sim$0.9 nm. Polymer probing predicts that between the intermediate and the main constriction the pore radius should be $\geq$0.9 nm. Crystallography demonstrates that at this part the channel pore has a widest bubble-like cavity.

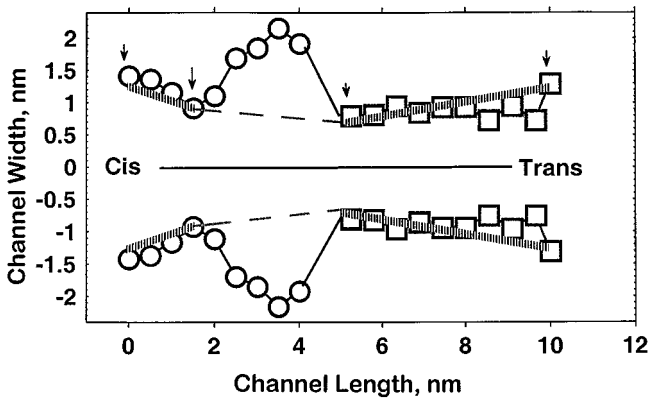

FIGURE 3 The apparent radius of the α-toxin channel pore along the pore axis from crystallographic and polymer probing studies. Channel length is shown in nanometers, starting from the *cis* opening. Symbols (○, □) joined by solid lines mark the approximate profile of the pore deduced from analysis of crystallographic data of Song et al. (1996) for Cap and Stem regions. Striped lines visualize the pore profile from polymer probing. Only relative positions of the two main constrictions could be deduced (see text), so their coordinates were taken to agree with crystallographic data. Arrows indicate key points of the pore geometry.

Thus, despite gross simplifications made in the interpretation (see Materials and Methods), polymer probing leads to very reasonable estimates of the pore structural features. It gives radii of the openings and two constrictions that are in good agreement with the crystallographic data. However, the apparent positions of the constrictions can be estimated only qualitatively.

Access resistance

The possible influence of channel access resistance on the sizes inferred from polymer probing (Bezrukov and Vodyanoy, 1993) was analyzed previously (Krasilnikov et al., 1998). It was shown that access resistance can change the experimentally observed amplitude of ion channel conductance variation versus hydrodynamic radius of polymers but does not significantly affect the principal features of the dependence and, thus, the deduced radii of crucial points of the channel lumen. In the case of the α-toxin channel under the conditions of our experiments, the access resistance is smaller than the channel resistance itself by $\sim$70 times. Therefore, the contribution of access resistance is negligible (see also Bezrukov et al., 1996).

Streaming potential

When a lipid bilayer modified by α-toxin separates two solutions, both containing 20% PEGs but of different molecular weights, a significant transmembrane potential is observed. The value of this potential depends on the osmotic pressure difference applied to the channel (Table 1). It can be seen that smaller polymer molecules that correspond to higher osmotic pressure differences (Parsegian et al., 1986) induce a higher transmembrane potential. The negative sign was always at the side containing the smaller PEG. This asymmetry-induced transmembrane potential was taken into account in calculations of g^{cis} and g^{trans}.

General considerations show that the observed transmembrane potential is a sum of at least three components: 1) streaming potential produced by solution flow through the channel, 2) potential generated by the salt gradient originating as a result of dilution (concentration) in an unstirred layer from the side of a higher (lower) osmotic pressure due to unidirectional flow of water through the lipid bilayer (Pohl et al., 1997, 1998), and 3) potential generated by a possible difference in the bulk KCl activity at opposite sides of the membrane. We have found that the addition of different PEGs used in our study changes the bulk KCl activity, but the difference is relatively small and cannot explain the observed value of the transmembrane potential. Thus contribution 3) is negligible. However, at this stage we cannot separate components 1) and 2). The sign and magnitude of the potential are consistent with a moderate anion selectivity of the α-toxin channel.

Influence of pH and high KCl concentrations on the hydrodynamic radius of PEG

In experiments with ion channels investigators often use large (≥1,0 M) concentrations of electrolytes to increase the signal-to-noise ratio. To evaluate the effects of titratable residues on ion channel properties, studies are also performed at different pH levels. For example, recently it was shown that the effect of pH is readily observed in the polymer exclusion experiments demonstrating an acidity-dependent shift in the apparent size of ion channels (Bezrukov and Kasianowicz, 1997). It is usually assumed that PEGs conserve their hydrodynamic characteristics at different salt concentrations and different pH levels.

Because no data about pH or 1:1 salt influence on hydrodynamic properties of PEG solutions could be found in the literature, we have studied their viscosity at different pH levels and salt concentrations. Our results demonstrate that the hydrodynamic radius of PEG only weakly increases, if at all, with pH. The radius of PEG3400 was determined to be equal to 1.62 ± 0.15 nm at pH 3.0 and to 1.65 ± 0.16 nm at pH 10.0.

The destabilizing effects of high concentrations of 2:2 electrolytes (like $MgSO_4$) on PEG solutions are well known (Lee and Lee, 1981). It is interesting to see if effects of this kind can be induced by high concentrations of 1:1 electrolytes. Measuring viscosity, we have established that an increase in KCl concentration induces a small decrease in the hydrodynamic radius of PEG. For PEG1500 and PEG4000 such dependencies are presented in Fig. 4. It appears that the larger the PEG molecular weight, the stronger is the effect of salt on its hydrodynamic radius.

PEG is not an inert probe of the α-toxin channel at high salt concentration

PEG-protein interactions were demonstrated about 10 years ago. For example, the thermal transition temperature for several proteins is lowered in the presence of PEGs (Lee and Lee, 1987; Arakawa and Timasheff, 1985). It was proposed that, at high concentrations, PEG could bind to hydrophobic sites of proteins. This assumption is supported by the fact that PEG is essentially nonpolar (Hammes and Schimmel, 1967; Ingham, 1977). Recent measurements (Sheth and Leckband, 1997) using the surface force apparatus showed a pronounced attraction between streptavidin and end-grafted PEG chains.

Remembering that the channel surfaces that are in contact with water (area of openings and the lumen) are usually a mosaic of charges and that PEG avoids charged species (Lee and Lee, 1981), it is plausible to assume that attraction of PEG to the ion channel lumen will increase with ion strength. The first direct evidence of this interaction was found recently (Bezrukov et al., 1996) from analysis of low-frequency spectral density of the α-toxin channel current noise in the presence of differently sized PEGs at 1 M NaCl. In polymer-probing experiments the attraction has to be seen as $F > 1.0$, especially in the presence of PEG at both sides of the membrane. Indeed, such an effect was repeatedly reported by several groups (e.g., Krasilnikov et al., 1997; Bezrukov et al., 1996).

Because of the importance of the subject we examined it further. The KCl concentration was raised to 1.0 M. Otherwise, the protocol of the experiments was identical to that used in the case of 0.1 M KCl. At the high concentration of permeant electrolyte considerable attraction between PEG and the channel could easily be seen (Fig. 5): the calculated values of the channel filling significantly exceed 1.0 for at least several PEGs. In agreement with the arguments above, an increase in salt concentration results in a decrease in the repulsion between charged groups of the channel and PEG, which makes the hydrophobic protein-PEG attraction stronger. Under these conditions the attraction between PEG and

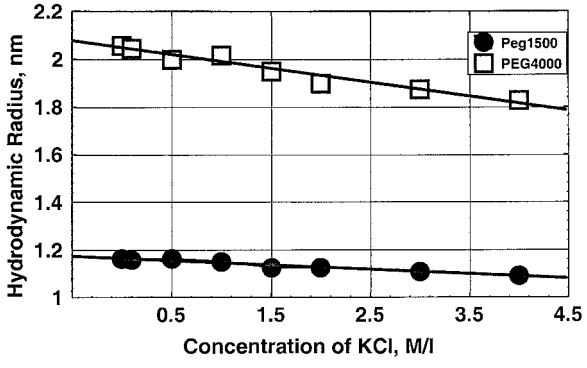

FIGURE 4 Dependence of the hydrodynamic radii of PEG1500 (●) and PEG4000 (□) on KCl concentration. Hydrodynamic radii were determined by viscometry as described elsewhere (Schultz and Solomon, 1961). Each value is the mean of five or six separate experiments. The error bars are equal to or smaller than the symbols used.

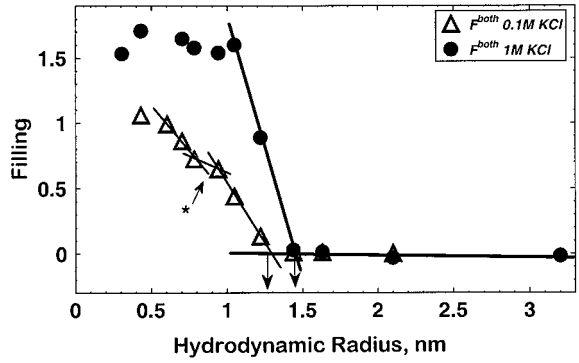

FIGURE 5 Dependence of F^{both} (symmetrical polymer addition) on polymer hydrodynamic radii in 0.1 M (△) and 1.0 M (●) KCl solutions. Arrows indicate the radii of the pore openings (~1.26 nm and ~1.44 nm) estimated in 0.1 M and 1.0 M KCl. 0.1 M KCl (△): Values of F^{both} in the presence of PEG3000, PEG3400, and PEG4600 were used to draw the horizontal line. The slope was fitted with two straight lines. To draw these two lines, the values of F^{both} for PEGs with radii ranging from 0.6 to 0.78 nm and from 0.94 to 1.22 nm, respectively, were used. 1.0 M KCl (●): Values of F^{both} in the presence of PEG3000, PEG3400, PEG4600, and PEG8000 were used to draw the horizontal line. The slope was fitted with one straight line, using the values of F^{both} for PEGs with radii ranging from 1.05 to 1.44 nm.

the α-toxin channel deforms the polymer-filling dependence on polymer hydrodynamic radius. As a result, the maximum size of the channel openings seems to exceed that obtained at 0.1 M KCl.

Interestingly, even at small salts (0.1 M KCl) symmetrical application of PEG yields a dependence of F^{both} on polymer weight, which shows only a hint of the intermediate invariant part (*an arrow with a star* in Fig. 5), while it is clearly seen in both the F^{cis} and F^{trans} dependencies (compare to Fig. 2). This observation emphasizes the difference between the methods of symmetrical and asymmetrical polymer probing. At symmetrical application the filling is less sensitive to the geometrical features of the channel pore.

On the physics of polymer partitioning into a channel pore

The qualitative picture of polymer partitioning into channel pores is intuitively clear: water-soluble polymers whose characteristic sizes are much smaller than pore diameters can easily enter them; large polymers are excluded from pores because of entropic or, for polymers comprising bulky monomers, for steric reasons. Quantitative description, however, is not that easy because a number of factors governing polymer distribution between the bulk and the pore are poorly understood. This holds true even in the case of symmetrical polymer application, when one is allowed to talk about equilibrium polymer partitioning.

The sharp dependence of the PEG partition coefficient on polymer molecular weight found for the α-toxin channel in several previous studies (Krasilnikov et al., 1992; Korchev et al., 1995; Bezrukov and Kasianowicz, 1997) could not be rationalized within the scaling theory approach (Bezrukov et al., 1996) and was attributed to polymer-pore attraction. Experimentally, this attraction manifested itself by an anomalously high level of low-frequency PEG-induced fluctuations and a pronounced PEG-induced reduction of channel conductance that exceeded the PEG-induced reduction of the bulk solution conductivity. In other words, polymer-pore attraction was made evident by a dramatic slowdown in PEG translocation within the pore and by significant accumulation of small PEGs in the pore (Bezrukov et al., 1996).

The results of the present study, which uses salt solutions of reduced concentration (0.1 M KCl versus 1 M salts in previous studies), do not indicate any substantial accumulation of small PEGs in the pore. As seen from Table 1, even for the smallest molecules used, the effect of PEG on channel conductance in this case never significantly exceeds its effect on bulk solution conductivity. Correspondingly, Fig. 5 shows that the filling factor saturates at a value close to unity, as compared to the filling factor at the high salt concentration (1 M KCl), where it goes well above 1.5. Nevertheless, polymer partitioning is again much sharper than scaling or hard-sphere approaches would predict for dilute polymer solutions.

In what follows we will analyze the equilibrium polymer partitioning rather than the filling factor. The calculation of the equilibrium polymer partitioning from the channel conductance relies only on assumption 1 (see Materials and Methods), at least for the pores that can be approximated by a regular circular cylinder. (Although the α-toxin channel pore does not fall into this category, it is clear that any deviation from the regular shape leads to a broadening of the transition between freely penetrating and completely sterically excluded polymers. We will see that this transition is actually anomalously sharp.) Experimental points for the polymer partitioning (Fig. 6) were calculated from the data in Table 1 (g^{both} and χ columns) as $p(w) = (g_0 - g(w))\chi_0/(\chi_0 - \chi(w))g_0$. This relationship follows from equation 3 of Bezrukov et al. (1996) if we neglect the effect of PEG on salt activity.

In the case of dilute polymer solutions their partition coefficient, defined as a ratio of polymer concentration in

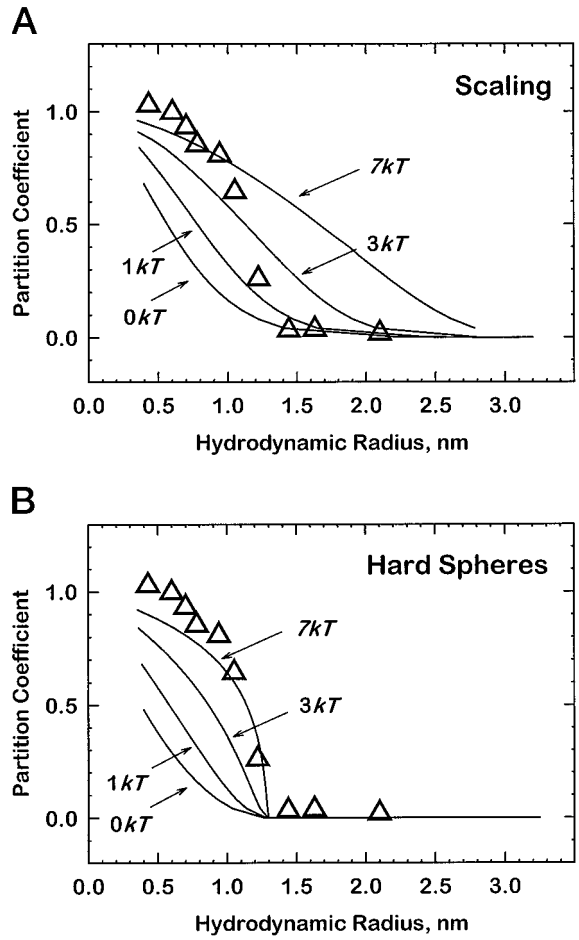

FIGURE 6 Polymer partitioning, p, for symmetrical PEG application as a function of polymer hydrodynamic radius measured for 0.1 M KCl bathing solution (△) in comparison with two theoretical predictions (——), which account for polymer-polymer repulsion. (*A*) The scaling approach; (*B*) the hard sphere approach. The different lines correspond to different excess free energies of polymer-polymer repulsion, Φ_0, used in Eqs. 8 and 10, correspondingly.

the pore, n_p, to polymer concentration in the bulk, n_b,, can be found from the polymer chemical potential balance. For the polymer chemical potential in the bulk we have

$$\mu_b = kT \ln n_b, \quad (1)$$

where k and T have their usual meanings of the Boltzmann constant and the absolute temperature. The chemical potential of the polymer in the channel pore or in any other water-filled cavity will differ from its value in the bulk, even in the absence of any specific interactions between monomers of the polymer molecule and the channel pore interior. This is due to configurational/translational limitations imposed by a cavity. A polymer molecule confined by the channel pore has lower entropy than its counterpart in the bulk.

In the scaling theory approach for a polymer molecule trapped in an infinite cylinder of radius R we can write (de Gennes, 1979; Grosberg and Khokhlov, 1994)

$$\mu_p^{SC} - kT \ln n_p \propto N(a/2R)^{5/3}, \quad (2)$$

where a is the segment (Kuhn's) length and N is the number of segments in the molecule. (While the result of the scaling theory used in Eq. 2 has been obtained for long pores with radii much smaller than the polymer gyration radius (strong confinement), a recent molecular dynamics simulation study by Boyd et al. (1996) shows an analogous dependence in the case where the radii of the pore and polymer are close (weak confinement). Fitting their results to Eq. 7, derived from Eq. 2 with N replaced by N^γ, we obtain $\gamma = 0.8$.) Using the relationship between polymer hydrodynamical radius and the chain length,

$$r_h \propto aN^{3/5}, \quad (3)$$

we obtain

$$\mu_p^{SC} = kT[\ln n_p + \beta(r_h/R)^{5/3}], \quad (4)$$

where β is a factor that cannot be evaluated within the framework of the scaling approach.

The partition coefficient is defined as the ratio of the equilibrium polymer concentration in the pore to that in bulk and is obtained by equating polymer chemical potentials, that is,

$$p \equiv \frac{n_p}{n_b} \quad (5)$$

at $\mu_p = \mu_b$. This gives the following simple expression for polymer partitioning:

$$p^{SC} = \exp[-\beta(r_h/R)^{5/3}]. \quad (6)$$

Fig. 6 *A* shows a comparison of experimental data for 0.1 M KCl and the predictions of Eq. 6 (the curve for $\Phi_0 = 0$). The pore is chosen to be a long cylinder of 1.3 nm radius, $\beta = 2.8$. It is seen that the scaling approach is not able to describe the sharpness of partition coefficient change with PEG weight, even in the case of a simple cylindrical geometry. It gives a much broader transition between complete exclusion and significant penetration than our experiment suggests.

PEG solutions at the 20% weight/volume concentration used in the present measurements can hardly be considered to be diluted. Indeed, osmotic pressure data for PEG (Parsegian et al., 1986) at these high concentrations suggest that polymers are no longer in the pure dilute regime. Rather, this concentration is very close to n^*, the characteristic concentration that separates the dilute from the semidilute regime. Polymer gyration volumes start to overlap, introducing significant entropic polymer-polymer repulsion. If we estimate an excess free energy, Φ_{ex}, due to this repulsion per polymer molecule for 20% PEG1000 solution, we end up with a value exceeding $1kT$. We use a deviation of polymer-induced osmotic pressure at this concentration (http://aqueous.labs.brocku.ca/osfile.html) from the osmotic pressure calculated from the ideal van't Hoff law, $\Delta\Pi$, and polymer gyration volume, v_g, to obtain $\Phi_{ex} \cong v_g\Delta\Pi$. Effective entropic repulsion between polymer molecules characterized by this energy can have significant consequences for polymer partitioning.

This question was recently explored in lattice computer simulations of semidilute polymer solutions in confined geometry by Wang and Teraoka (1997). It was shown that partitioning of model "polymers" with $N = 100$ into a narrow slit could be enhanced by a factor of ~20 in comparison to dilute solutions when the polymer concentration in the bulk approached n^*.

To introduce this effect in our consideration, we will assume the simplest possible relationship between excess free energy of polymer-polymer repulsion and polymer concentration: $\Phi_{ex} \propto n$, that is, basically accounting for the first virial coefficient only. We checked this assumption against simulation data by Wang and Teraoka and, by adjusting parameter Φ^* in $\Phi_{ex} = \Phi^*(n/n^*)$, we obtained a reasonable agreement for $\Phi^* = (5–7)kT$. For simplicity, we will also ignore the dependence of Φ_{ex} on the polymer molecular weight.

We write the polymer-polymer entropic repulsion correction to chemical potential in the form

$$\mu' = \mu + (\Phi^*/n^*)n, \quad (7)$$

where μ is given by Eqs. 1 and 4 and n is n_b or n_p, correspondingly. Condition $\mu_p = \mu_b$ then gives the following equation for the partition coefficient:

$$p^{SC} \exp[(\Phi_0 p^{SC} - \Phi_0)/kT] = \exp[-\beta(r_h/R)^{5/3}], \quad (8)$$

where $\Phi_0 = (\phi^*/n^*)n_b$ is an excess free energy of polymer-polymer repulsion at the bulk concentration.

Fig. 6 *A* shows that at an increased repulsion (higher Φ_0) the partition coefficient, p^{SC}, is mostly shifted to higher polymer weights without changing its sharpness appreciably. All curves are calculated for $R = 1.3$ nm and $\beta = 2.8$. Using β as an adjustable parameter improves fitting; but, even at $\Phi_0 = 7kT$, it is impossible to choose a value of β

that would generate a curve describing, within the data accuracy (the size of symbols in the figure), more than two points in the dispersion region of 0.75 nm $> r >$ 1.7 nm. Thus the scaling approach does not allow us to rationalize our data, even when polymer-polymer repulsion is included in the model.

For an alternative model of partitioning, the hard sphere partitioning (e.g., Colton et al., 1975; Boyd et al., 1996), the corresponding chemical potential for dilute solutions can be written as

$$\mu_p^{HS} = kT[\ln n_p - \ln(1 - r/R)^2], \quad (9)$$

where r is the radius of a sphere. Assuming that for a sphere $r = r_h$ and introducing polymer-polymer repulsion by Eq. 7, from Eq. 5 we have

$$p^{HS} \exp[(\Phi_0 p^{HS} - \Phi_0)/kT] = (1 - r_h/R)^2, \quad (10)$$

which, for $\Phi_0 = 0$, reduces to the following familiar result (e.g., Casassa, 1971):

$$p^{HS} = (1 - r_h/R)^2. \quad (11)$$

Fig. 6 *B* represents a comparison of our experimental results with the partition coefficient calculated according to Eq. 10 at different repulsion energies at $R = 1.3$ nm. It is seen that the increasing Φ_0 sharpens the dependence of the hard sphere partition coefficient, p^{HS}, on polymer molecular weight to approach the sharpness of experimentally measured partitioning. It does not describe partitioning of the smallest PEG used, which may suggest some polymer-pore attraction unaccounted for by the present treatment.

Here we disregarded the dependence of Φ_0 on molecular weight, which is a monotonously increasing function. The larger polymer chains are pushed harder into the pore than the smaller ones, even at conserved monomeric concentration. It is clear, however, that such a dependence will further broaden the transition between penetration and exclusion in the case of p^{SC}. As for p^{HS}, it is not going to be changed much because the size cutoff for hard spheres is sharp. Hard spheres with $r > R$ do not penetrate at all.

For unknown reasons, highly flexible PEG molecules (with a Kuhn length of only several Angstroms) in experiments with the α-toxin channel phenomenologically behave like hard spheres rather than "soft" particles of the scaling approach. But those must be hard spheres with additional particle-particle repulsion due to the nonideality of the bathing solution.

To understand the actual situation better, more detailed information concerning partitioning mechanisms is needed. The most important issue concerns possible polymer-pore interactions that are not explicitly seen in the averaged channel behavior studied in the present paper. As a next step, we plan to perform dynamic studies of polymer partitioning, using time analysis of polymer-induced conductance fluctuations (Bezrukov et al., 1994) at the level of a single α-toxin channel. However, already at this stage, it is quite clear that probing ion channel pores with asymmetrically applied polymers (Krasilnikov et al., 1998) is a promising structural tool for examining ion channels in their functional states.

We are grateful to V. Adrian Parsegian, Sasha Berezhkovskii, and Donald Rau for enlightening discussions and for reading the manuscript. We thank N. Grineva for skilled technical assistance and Drs. H. Bayley and K. D. Hungerer for the gift of α-toxin.

This study was partially supported by the Conselho National de Desenvolvimento Cientifico e Tecnologico (Brazil).

REFERENCES

Arakawa, T., and S. N. Timasheff. 1985. Mechanism of poly(ethylene glycol) interaction with proteins. *Biochemistry.* 24:6756–6762.

Berezhkovskii, A. M., S. M. Bezrukov, D. J. Bicout, and G. H. Weiss. 1999. The influence of polymer on the diffuision of a spherical tracer. *J. Chem. Phys.* 111:5641–5644.

Bezrukov, S. M., and J. J. Kasianowicz. 1997. The charge state of an ion channel controls neutral polymer entry into its pore. *Eur. Biophys. J.* 26:471–476.

Bezrukov, S. M., and I. Vodyanoy. 1993. Probing alamethicin channels with water-soluble polymers. Effect on conductance of channel states. *Biophys. J.* 64:16–25.

Bezrukov, S. M., I. Vodyanoy, R. A. Brutyan, and J. J. Kasianowicz. 1996. Dynamics and free energy of polymers partitioning into a nanoscale pore. *Macromolecules.* 29:8517–8522.

Bezrukov, S. M., I. Vodyanoy, and V. A. Parsegian. 1994. Counting polymers moving through a single ion channel. *Nature.* 370:279–281.

Bhakdi, S., M. Muhly, and R. Fussle. 1984. Correlation between toxin binding and hemolytic activity in membrane damage by staphylococcal α-toxin. *Infect. Immun.* 46:318–323.

Boyd, R. H., R. R. Chance, and G. Ver Strate. 1996. Effective diment ions of oligomers in size exclusion chromatography. A molecular dynamics simulation study. *Macromolecules.* 29:1182–1190.

Bullock, J. O., and E. R. Kolen. 1995. Ion selectivity of colicin E1:III. Anion permeability. *J. Membr. Biol.* 144:131–145.

Casassa, E. F. 1971. Theoretical models for peak migration in gel permeation chromatography. *J. Phys. Chem.* 75:3929–3939.

Colton, C. K., C. N. Satterfield, and C.-J. Lai. 1975. Diffusion and partitioning of macromolecules within finely porous glass. *AIChE J.* 21:289–298.

Couper, A., and R. F. T. Stepto. 1969. Diffusion of low-molecular weight poly(ethylene oxide) in water. *Trans. Faraday Soc.* 65:2486–2496.

Czajkowsky, D. M., S. Sheng, and Z. Shao. 1998. Staphylococcal α-hemolysin can form hexamers in phospholipid bilayers. *J. Mol. Biol.* 276:325–330.

de Gennes, P.-G. 1979. Scaling Concepts in Polymer Physics. Cornell University Press, Ithaca, New York.

Desai, S. A., and R. L. Rosenberg. 1997. Pore size of the malaria parasite's nutrient channel. *Proc. Natl. Acad. Sci. USA.* 94:2045–2049.

Eler, H. 1972. Statistical Method for Approaching. AINP Report P11–6816. Dubna AINP Publishers, Moscow. 27.

Gouaux, J. E., O. Braha, M. R. Hobaugh, L. Song, S. Cheley, C. Shustak, and H. Bayley. 1994. Subunit stoichiometry of staphylococcal alpha-hemolysin in crystals and on membranes: a heptameric transmembrane pore. *Proc. Natl. Acad. Sci. USA.* 91:12828–12831.

Grey, G. S., and M. Kehoe. 1984. Primary sequence on the alpha-toxin gene from *Staphylococcus aureus* Wood 46. *Infect. Immun.* 46:615–618.

Grosberg, A. Yu., and A. R. Khokhlov. 1994. Statistical Physics of Macromolecules. AIP Press, New York.

Hammes, G. G., and P. R. Schimmel. 1967. An investigation of water-urea and water-urea-polyethylene glycol interactions. *J. Am. Chem. Soc.* 89:442–446.

Hille, B. 1992. Ionic Channels of Excitable Membranes. Sinauer Associates, Sunderland, MA.

Ingham, K. C. 1977. Polyethylene glycol in aqueous solution: solvent perturbation and gel filtration studies. *Arch. Biochem. Biophys.* 184: 59–68.

Jonas, D., I. Walev, T. Berger, M. Liebetrau, and S. Bhakdi. 1994. Novel path to apoptosis: small transmembrane pores created by staphylococcal alpha-toxin in T lymphocytes evoke internucleosomal DNA degradation. *Infect. Immun.* 62:1304–1312.

Kaulin, Y. A., L. V. Schagina, S. M. Bezrukov, V. V. Malev, A. M. Feigin, J. Y. Takemoto, J. H. Teeter, and J. G. Brand. 1998. Cluster organization of ion channels formed by the antibiotic syringomycin E in bilayer lipid membranes. *Biophys. J.* 74:2918–2925.

Korchev, Y. E., C. L. Bashford, C. M. Alder, J. J. Kasianowicz, and C. A. Pasternak. 1995. Low conductance states of a single ion channel are not "closed." *J. Membr. Biol.* 147:233–239.

Krasilnikov, O. V., J. B. Da Cruz, L. N. Yuldasheva, and R. A. Nogueira. 1998. A novel approach to study the geometry of the water lumen of ion channels: colicin Ia channels in planar lipid bilayers. *J. Membr. Biol.* 161:83–92.

Krasilnikov, O. V., P. G. Merzlyak, L. N. Yuldasheva, R. K. Azimova, and R. A. Nogueira. 1997. Pore-forming properties of proteolytically nicked staphylococcal α-toxin. The ion channel in planar lipid bilayer membranes. *Med. Microbiol. Immunol.* 186:53–61.

Krasilnikov, O. V., and R. Z. Sabirov. 1989. Ion transport through channels formed in lipid bilayers by *Staphylococcus aureus* α-toxin. *Gen. Physiol. Biophys.* 8:213–222.

Krasilnikov, O. V., R. Z. Sabirov, V. I. Ternovsky, P. G. Merzliak, and J. N. Muratkhodjaev. 1992. A simple method for the determination of the pore radius of ion channels in planar lipid bilayer membranes. *FEMS Microbiol. Immunol.* 105:93–100.

Krasilnikov, O. V., R. Z. Sabirov, V. I. Ternovsky, P. G. Merzliak, and B. A. Tashmukhamedov. 1988. Structure of ion channels induced by α-toxin from *Staphylococcus aureus. Gen. Physiol. Biophys.* 7:467–473.

Krasilnikov, O. V., V. I. Ternovsky, Yu. M. Musaev, and B. A. Tashmukhamedov. 1980. Influence of staphylotoxin on conductance of bilayer phospholipid membranes. *Dokl. Akad. Nauk UzSSR.* N7:66–68.

Krasilnikov, O. V., V. I. Ternovsky, and B. A. Tashmukhamedov. 1981. Properties of ion channels induced by alpha-staphylotoxin in bilayer lipid membranes. *Biofisica.* 26:271–275.

Kuga, S. 1981. Pore size distribution analysis of gel substances by size exclusion chromatography. *J. Chromatogr.* 206:449–461.

Lee, J. C., and L. L. Lee. 1981. Preferential solvent interactions between proteins and polyethylene glycols. *J. Biol. Chem.* 256:625–631.

Lee, L. L., and J. C. Lee. 1987. Thermal stability of proteins in the presence of poly(ethylene)glycols. *Biochemistry.* 26:7813–7819.

Menestrina, G. 1986. Ion channels formed by *Staphylococcus aureus* α-toxin. Voltage-dependent inhibition by divalent and trivalent cations. *J. Membr. Biol.* 90:177–190.

Mueller, P., D. O. Rudin, H. T. Tien, and W. C. Wescott. 1963. Methods for the formation on single bimolecular lipid membranes in aqueous solution. *J. Phys. Chem.* 67:534–535.

Parsegian, V. A., S. M. Bezrukov, and I. Vodyanoy. 1995. Watching small molecules move: interrogating ionic channels using neutral solutes. *Biosci. Rep.* 15:503–514.

Parsegian, V. A., R. P. Rand, N. L. Fuller, and D. C. Rau. 1986. Osmotic stress for the direct measurement of intermolecular forces. *Methods Enzymol.* 127:400–416.

Pohl, P., S. M. Saparov, and Y. N. Antonenko. 1997. The effect of a transmembrane osmotic flux on the ion concentration distribution in the immediate membrane vicinity measured by microelectrodes. *Biophys. J.* 72:1711–1718.

Pohl, P., S. M. Saparov, and Y. N. Antonenko. 1998. The size of the unstirred layer as a function of the solute diffusion coefficient. *Biophys. J.* 75:1403–1409.

Sabirov, R. Z., O. V. Krasilnikov, V. I. Ternovsky, and P. G. Merzliak. 1993. Relation between ionic channel conductance and conductivity of media containing different nonelectrolytes. The novel method of pore size determination. *Gen. Physiol. Biophys.* 12:95–111.

Sabirov, R. Z., O. V. Krasilnikov, V. I. Ternovsky, P. G. Merzliak, and J. N. Muratkhodjaev. 1991. Influence of some nonelectrolytes on conductivity of bulk solution and conductance of ion channels. Determination of pore radius from electric measurements. *Biol. Membr.* 8:280–291.

Schultz, S. G., and A. K. Solomon. 1961. Determination of the effective hydrodynamic radii of small molecules by viscometry. *J. Gen. Physiol.* 44:1189–1199.

Sheth, S. R., and D. Leckband. 1997. Measurements of attractive forces between proteins and end-grafted poly(ethylene glycol) chains. *Proc. Natl. Acad. Sci. USA.* 94:8399–8404.

Song, L., M. R. Hobaugh, C. Shustak, S. Cheley, H. Bayley, and J. E. Gouaux. 1996. Structure of staphylococcal α-hemolysin, a heptameric transmembrane pore. *Science.* 274:1859–1866.

Ternovsky, V. I., and G. N. Berestovsky. 1998. Effective diameter and structural organization of reconstituted calcium channels from the Characeae algae Nitellopsis. *Membr. Cell Biol.* 12:79–88.

Tomita, T., M. Watanabe, and T. Yasuda. 1992. Influence of membrane fluidity on assembly of *Staphylococcus aureus* α-toxin, a channel-forming protein, in liposome membrane. *J. Biol. Chem.* 267: 13391–13397.

Valeva, A., A. Weisser, B. Walker, M. Kehoe, H. Bayley, S. Bhakdi, and M. Palmer. 1996. Molecular architecture of a toxin pore: a 15-residue sequence lines the transmembrane channel of Staphylococcal alpha-toxin. *EMBO J.* 15:1857–1864.

Vecsey-Semjen, B., C. Lesieur, R. Mollby, and F. G. van der Goot. 1997. Conformational changes due to membrane binding and channel formation by staphylococcal alpha-toxin. *J. Biol. Chem.* 272:5709–5717.

Villarroel, A., N. Burnashev, and B. Sakmann. 1995. Dimensions of the narrow portion of a recombinant NMDA receptor channel. *Biophys. J.* 68:866–875.

Vodyanoy, I., and S. M. Bezrukov. 1992. Sizing of an ion pore by access resistance measurement. *Biophys. J.* 62:10–11.

Walev, I., E. Martin, D. Jonas, M. Mohamadzadeh, W. Miller-Klieser, L. Kunz, and S. Bhakdi. 1993. Staphylococcal alpha-toxin kills human keratinocytes by permeabilizing the plasma membrane for monovalent ions. *Infect. Immun.* 61:4972–4979.

Wang, Y., and I. Teraoka. 1997. Computer simulation of semidilute polymer solutions in confined geometry: pore as a microscopic probe. *Macromolecules.* 30:8473–8477.

Zimmerberg, J., and V. A. Parsegian. 1986. Polymer inaccessible volume changes during opening and closing of a voltage-dependent ionic channel. *Nature.* 323:36–39.